Magn Reson Med Sci 2020; 19; 227–234
doi:10.2463/mrms.mp.2019-0049
Published Online: October 15, 2019

MAJOR PAPER

Prediction of Hypoxia in Brain Tumors Using a Multivariate Model Built from MR Imaging and ^{18}F-Fluorodeoxyglucose Accumulation Data

Yukie Shimizu[1], Kohsuke Kudo[2,3*], Hiroyuki Kameda[2], Taisuke Harada[2], Noriyuki Fujima[2], Takuya Toyonaga[4], Khin Khin Tha[2,3], and Hiroki Shirato[1,3]

Purpose: The aim of this study was to generate a multivariate model using various MRI markers of blood flow and vascular permeability and accumulation of ^{18}F-fluorodeoxyglucose (FDG) to predict the extent of hypoxia in an ^{18}F-fluoromisonidazole (FMISO)-positive region.

Methods: Fifteen patients aged 27–74 years with brain tumors (glioma, $n = 13$; lymphoma, $n = 1$; germinoma, $n = 1$) were included. MRI scans were performed using a 3T scanner, and dynamic contrast-enhanced (DCE) perfusion and arterial spin labeling images were obtained. K_{trans} and V_p maps were generated using the DCE images. FDG and FMISO positron emission tomography scans were also obtained. A model for predicting FMISO positivity was generated on a voxel-by-voxel basis by a multivariate logistic regression model using all the MRI parameters with and without FDG. Receiver-operating characteristic curve analysis was used to detect FMISO positivity with multivariate and univariate analysis of each parameter. Cross-validation was performed using the leave-one-out method.

Results: The area under the curve (AUC) was highest for the multivariate prediction model with FDG (0.892) followed by the multivariate model without FDG and univariate analysis with FDG and K_{trans} (0.844 for all). In cross-validation, the multivariate model with FDG had the highest AUC (0.857 ± 0.08) followed by the multivariate model without FDG (0.834 ± 0.119).

Conclusion: A multivariate prediction model created using blood flow, vascular permeability, and glycometabolism parameters can predict the extent of hypoxia in FMISO-positive areas in patients with brain tumors.

Keywords: *brain tumors, hypoxia, magnetic resonance imaging, positron emission tomography, prediction model*

Introduction

Hypoxia has been reported to be associated with cell proliferation and survival.[1–3] Therefore, oxygen metabolism is an important factor in assessment of various types of tumors. An imbalance in oxygen demand and supply supposedly occurs in highly proliferative tumors, leading to hypoxic conditions that induce expression of several genes involved in changes in metabolism fit for the hypoxic condition.[1,2,4] Clinically, hypoxia in tumors is associated with resistance to treatment and a poor prognosis.[5–7]

^{18}F-fluoromisonidazole (FMISO) positron emission tomography (PET), whereby hypoxic regions within a tumor can be identified by accumulation of FMISO in areas with a low partial pressure of oxygen, is now recognized as the gold standard for assessment of tumor hypoxia and has been used clinically in several types of tumors, including glioma.[5,7,8] However, ^{18}F-FMISO PET has limited availability, and MRI and ^{18}F-fluorodeoxyglucose (^{18}F-FDG) PET are more readily accessible at most hospitals. MRI is now capable of evaluating vascular characteristics such as perfusion and permeability of vessels, so assessment of MRI parameters and accumulation of FDG would be useful for predicting FMISO positivity.

Tumor oxygenation is thought to be mediated by changes in blood flow, vascular density or blood volume, and microvessel geometry, all of which can be measured using

[1]Department of Radiation Medicine, Hokkaido University Graduate School of Medicine, Hokkaido, Japan
[2]Department of Diagnostic and Interventional Radiology, Hokkaido University Hospital, Hokkaido, Japan
[3]Global Station for Quantum Medical Science and Engineering, Global Institution for Collaborative Research and Education, Hokkaido University, Hokkaido, Japan
[4]Department of Nuclear Medicine, Hokkaido University Graduate School of Medicine, Hokkaido, Japan
*Corresponding author, Department of Diagnostic Imaging, Hokkaido University Graduate School of Medicine and Faculty of Medicine, N15 W7, Kita-ku, Sapporo, Hokkaido 060-8638, Japan, Phone: +81-11-706-7779, Fax: +81-11-706-7408, E-mail: kkudo@huhp.hokudai.ac.jp

Received: March 29, 2019 | Accepted: August 14, 2019

dynamic susceptibility contrast (DSC) or dynamic contrast-enhanced (DCE) MRI perfusion techniques.[9–13] Blood flow and blood volume are quantified by DSC. Blood volume and vascular permeability are quantified by DCE as V_p and K_{trans}, respectively.

An earlier study that investigated the relationship between ^{18}F-FMISO PET and MRI findings in glioblastoma found that uptake of FMISO was associated with cerebral blood volume in that there was a positive correlation between the extent of hypoxia within a tumor and hypervascularity of the tumor and between maximum ^{18}F-FMISO uptake and blood volume.[14] It was also suggested that tumor hypoxia and hypervascularization were more frequent and intense in contrast-enhanced areas of glioblastomas that are thought to indicate abnormal vascular permeability zones caused by breakdown of the blood–brain barrier, although Gerstner et al. did not perform a quantitative analysis of permeability using DCE in their study. Another study showed a significant association of greater accumulation of ^{18}F-FMISO and K_{trans} with shorter survival but not of uptake of ^{18}F-FMISO with permeability markers.[3]

In addition to vascularity, glycometabolism, assessed by extent of accumulation of FDG, is widely recognized as an indicator of a highly proliferative tumor. FDG is thought to be a marker of various aspects of tumor biology, resulting in an FDG-avid volume that is generally larger than that with ^{18}F-FMISO, although the hypoxic area shown by FMISO is not always included in the FDG-avid area.[15]

Therefore, we hypothesized that accumulation of ^{18}F-FMISO in brain tumors can be predicted by a multivariate model using MRI parameters and accumulation of FDG. The aim of this study was to generate a multivariate model that can predict the likelihood of FMISO positivity.

Materials and Methods

Subjects

Patients who were referred to our hospital for preoperative evaluation of a brain tumor between May 2015 and June 2016 were prospectively enrolled. The study inclusion criteria were as follows: suggestion of a brain tumor greater than 1 cm in diameter observed on MRI; scheduled to undergo ^{18}F-FMISO PET, and age 20 years or older. Patients were excluded if they had any contraindications to MRI or gadolinium contrast agents, were pregnant or breastfeeding, or had renal dysfunction. In our research plan, histology of the tumor was not limited in the text. However, the indication of ^{18}F-FMISO PET was decided by the surgeons, and clinically limited to the following three occasions: (1) highly suspected malignant tumor, (2) need for differentiating from malignant tumor, (3) observation of treated malignant tumor, or examination of possible malignant transformation of low grade glioma. Therefore, patients with apparently benign tumor such as meningioma or schwannoma were not included because they did not undergo ^{18}F-FMISO PET during the study duration.

Fifteen patients (seven female, eight male; aged 27–74 years) were finally eligible for the study (Table 1). Thirteen of these patients had a histopathological diagnosis of glioma. Three of the 13 patients had already undergone surgery and had residual tumor (grade 2 oligodendroglioma, $n = 1$; grade 2 oligoastrocytoma, $n = 1$; grade 4 glioblastoma, $n = 1$) and the

Table 1 Patient demographics and clinical and imaging characteristics

Case	Age (years)	Sex	Diagnosis	Accumulation of FMISO	Total voxel number
1	47	M	Glioblastoma	Positive	6947
2	70	M	Glioblastoma	Positive	13794
3	56	M	Glioblastoma	Positive	20503
4	57	M	Glioblastoma	Positive	6266
5	71	F	Glioblastoma	Positive	18793
6	27	F	Glioblastoma	Positive	13771
7	57	F	Anaplastic oligoastrocytoma	Positive	4123
8	29	F	Germinoma	Positive	2484
9	38	M	Glioblastoma	Positive	24319
10	73	F	Anaplastic astrocytoma	Positive	5811
11	67	F	Anaplastic astrocytoma	Positive	2573
12	33	M	Residual oligodendroglioma	Negative	2996
13	74	M	Residual glioblastoma	Negative	8893
14	74	M	Lymphoma	Negative	19453
15	39	F	Residual oligoastrocytoma	Negative	57403

FMISO, ^{18}F-fluoromisonidazole.

remaining 10 gliomas were high-grade and untreated, comprising seven grade 4 glioblastomas, two grade 3 anaplastic astrocytomas, and one grade 3 anaplastic oligoastrocytoma. Two of the 15 patients had tumors other than glioma (malignant lymphoma, $n = 1$; germinoma, $n = 1$). As stated above, two cases were histopathologically diagnosed as "oligoastrocytoma, which is not shown in the 2016 World Health Organization Classification of Tumors of the Central Nervous System, because their diagnoses were made before the revision of the World Health Organization classification.

All patients underwent MRI, including fluid-attenuated inversion recovery (FLAIR) imaging, DCE perfusion, and arterial spin labeling (ASL), as well as ^{18}F-FMISO PET and ^{18}F-FDG PET imaging. The interval between scans was <10 days.

Magnetic resonance imaging

All MRI scans were obtained using a 3T unit (Trillium Oval; Hitachi, Ltd., Tokyo, Japan) with a 15-channel head coil. DCE perfusion was performed using a 3D gradient echo sequence. The scan parameters included a flip angle of 10°, a TE of 3.0 ms, a TR of 5.4 ms, a FOV of 240 mm, a slab thickness of 150 mm, a section thickness of 5 mm, and an acquisition matrix of 256 × 128. After five phases of baseline acquisition, gadolinium 0.1 mmol/kg was injected intravenously as a bolus at a rate of 3 mL/s: meglumine gadopentetate, gadobutrol (Bayer Yakuhin, Ltd., Osaka, Japan), meglumine gadoterate (Guerbet Japan, Ltd., Tokyo, Japan), or gadodiamide (Daiichi Sankyo Co., Ltd., Tokyo, Japan). The total scan time was 3 min and 50 s. The ASL images were acquired using a pulsed continuous ASL sequence. The scan parameters included a flip angle of 90°, a TE of 15 ms, a TR of 4500 ms, a FOV of 240 mm, a section thickness of 6 mm, a slab thickness of 156 mm, an acquisition matrix of 64 × 50, and a post-labeling delay (PLD) of 1500 ms. Although PLD was set shorter than that recommended by the International Society for Magnetic Resonance in Medicine (ISMRM) perfusion study group and the European consortium for ASL in dementia,[16] we considered it adequate because magnetic resonance or computed tomography angiography showed no stenosis in the major head and neck arteries of the patients enrolled in this study. Conventional axial T_1-, T_2-weighted, and axial fluid-attenuated inversion recovery (FLAIR) sequences were acquired at the same time. The scan parameters for the FLAIR sequence included a flip angle of 90°, a TE of 162 ms, a TR of 12000 ms, an inversion time of 2770 ms, a FOV of 240 mm, a section thickness of 5 mm, and an acquisition matrix of 320 × 336.

Positron emission tomography

A Biograph 64 PET–CT scanner (Asahi-Siemens Medical Technologies Ltd., Tokyo, Japan), ECAT EXACT HR+ PET scanner (Asahi-Siemens Medical Technologies Ltd.), or Gemini TF64 TOF-PET/CT scanner (Hitachi Medical Corporation Ltd., Tokyo, Japan) was used. All PET–CT scanners were operated in 3D mode.

^{18}F-FMISO PET

The patients were not required to fast prior to ^{18}F-FMISO PET scanning. Static PET scanning was started 4 h after intravenous injection of 5 MBq/kg of FMISO. CT was performed for attenuation correction followed by a 10-min emission acquisition. Attenuation-corrected radioactivity images were reconstructed using either the filtered back projection method (ECAT EXACT HR+ and Biograph 64) or the ordered subset expectation maximization method (Gemini TF64) with a Hann filter of 4 mm full width at half maximum.

^{18}F-FDG PET

The patients fasted for more than 6 h before undergoing the ^{18}F-FDG PET examination. The static PET images were acquired 1 h after intravenous injection of FDG (4.5 MBq/kg). The acquisition time and image reconstruction for FDG PET were the same as those for FMISO PET.

Image processing and analysis

The DCE images were post-processed for analysis of permeability using Olea Sphere version 2.3 (Olea Medical, La Ciotat, France). The arterial input function was automatically generated for a chosen section of either of the internal, middle, or anterior cerebral arteries. An extended Tofts model was used to generate V_p and K_{trans} maps.

Registration of the MR and PET images was performed using SPM12 software (Wellcome Trust Centre, London, United Kingdom). The registered images, including ^{18}F-FMISO-PET and ^{18}F-FDG-PET images, FLAIR images, V_p and K_{trans} maps, and ASL images were then imported into PET Research Assistant software (an in-house software, unpublished). ROIs were then created for measurement of the normal standard values described below. The entire tumor volume was defined on the FLAIR images. Spherical ROIs (with a diameter of 10 mm) were placed in the normal white matter on the other side of the tumor (Fig. 1a). The area with high signal (>1.2 times the normal white matter value) surrounding the enhanced region on T_1-weighted images performed after DCE perfusion was determined to be the entire tumor volume. Spherical ROIs (with a diameter of 10 mm) were placed diffusely in the both hemispheres of the cerebellum on the FMISO images; the average values were used for the standard FMISO uptake (Fig. 1b). FMISO positivity was defined as the area where the lesion to cerebellum ratio was >1.3.

Spherical ROIs were also placed in the gray matter on the opposite side of the tumor on the ASL and FDG images (Fig. 1c); the averages were used as the standard ASL and FDG values. The values relative to the standard values were analyzed further. Regarding ASL, quantitative cerebral blood flow (CBF) maps were not created in this study, and just relative values were used. The absolute K_{trans} and V_p values were analyzed quantitatively.

The model for prediction of FMISO positivity was generated on a voxel-by-voxel basis by multivariate logistic regression analysis of the FDG, ASL, K_{trans}, and V_p values of

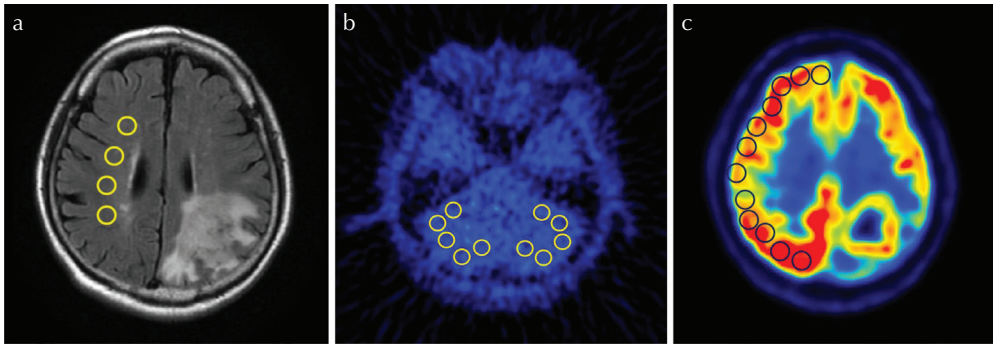

Fig. 1 Placement of regions of interest for measurement of normal standard values. Spherical regions of interest placed in the normal white matter on the other side of the tumor for measurement of the normal fluid-attenuated inversion recovery (FLAIR) value (**a**), placed diffusely in both hemispheres of the cerebellum for standard ^{18}F-fluoromisonidazole (FMISO) uptake (**b**), and placed in the gray matter on the opposite side of the tumor to standardize arterial spin labelling and ^{18}F-fluorodeoxyglucose values (**c**).

the voxels using JMP software (SAS Institute Inc., Cary, NC, USA). We also attempted to generate the model without FDG, i.e., using only MRI parameters (ASL, K_{trans}, and V_p).

Eleven of the 15 patients had FMISO-positive lesions and four (three postoperative gliomas and one lymphoma) patients did not show significant accumulation of FMISO (Table 1). Therefore, data for all 15 patients could be used to generate the multivariate prediction model, which was validated using the 11 cases with significant accumulation of FMISO.

We generated a prediction map showing the probability of positive accumulation of FMISO based on the calculated formula using the free Perfusion Mismatch Analyzer software package (version 5.2.0.0) (Acute Stroke Imaging Standardization Group, Japan).

Statistical analysis

Receiver-operating characteristic (ROC) curve analysis was used to assess the accuracy in detecting FMISO positivity in the 11 patients with FMISO-positive voxels. The ROC analysis was performed for the generated multivariate logistic regression models with or without FDG, and also for univariate analyses with FDG, ASL, K_{trans}, and V_p. The multivariate prediction model was generated and the ROC curve analysis was performed using the voxels for all 15 patients. Leave-one-out cross-validation was performed for each of the 11 patients (e.g., one patient was excluded from generation of the multivariate prediction model but the ROC curve analysis did include this patient).

Pairwise comparison of the average area under the curve (AUC) between the multivariate prediction models and the univariate analyses was performed using the Student-Newman-Keuls method. A P-value <0.05 was considered statistically significant.

Results

The numbers of the voxels for each case are shown in Table 1. The AUC for all 15 patients and the average AUCs for the cross-validation of FDG, ASL, K_{trans}, V_p, and the model with and without FDG are shown in Table 2. The AUC that included all 15 patients was highest in the multivariate prediction model with FDG (0.892) followed by the multivariate prediction model without FDG and univariate analysis of FDG and K_{trans} (0.844 for all).

Table 2 Results of receiver-operating characteristic curve analysis

Case	Multivariate prediction model		Univariate analysis			
	With FDG	Without FDG	FDG	ASL	K_{trans}	V_p
All 15 patients	0.892	0.844	0.844	0.830	0.844	0.727
Cross-validation						
1	0.975	0.957	0.966	0.944	0.968	0.980
2	0.900	0.886	0.807	0.875	0.924	0.869
3	0.777	0.737	0.835	0.725	0.852	0.775
4	0.820	0.776	0.782	0.792	0.728	0.661
5	0.961	0.899	0.972	0.845	0.953	0.919
6	0.970	0.884	0.952	0.880	0.821	0.694
7	0.719	0.731	0.702	0.710	0.759	0.722
8	0.824	0.773	0.666	0.804	0.195	0.161
9	0.843	0.815	0.830	0.790	0.869	0.813
10	0.853	0.905	0.702	0.182	0.986	0.188
11	0.787	0.810	0.612	0.567	0.847	0.955
Mean	0.857	0.834	0.802	0.738	0.809	0.703
SD	0.081	0.072	0.119	0.200	0.210	0.268

FDG, ^{18}F-fluorodeoxyglucose; SD, standard deviation; ASL, arterial spin labeling.

In the cross-validation, the average AUC for the multivariate prediction model with FDG was the highest and was significantly higher than for univariate analysis of ASL (0.738 ± 0.200, $P = 0.018$) and V_p (0.703 ± 0.268, $P = 0.037$). There were no significant differences between the multivariate prediction model with FDG and univariate analysis of

K_{trans} (0.809 ± 0.210, P = 0.366) or FDG (0.802 ± 0.119, P = 0.064). The average AUC for the multivariate prediction model without FDG was the second highest (0.834 ± 0.072); however, there were no significant differences for the other variables (P > 0.05). There were no ASL, K_{trans}, and V_p outliers in the multivariate prediction models with or without FDG seen in the univariate analysis (Fig. 2).

The multivariate prediction map for one patient with glioblastoma (case 6) is presented in Fig. 3 with its true ^{18}F-FMISO map and FLAIR image. FMISO positivity was predicted using the following equation (derived from the patient's complete data set):

$$\text{FMISO}\ (P) = \frac{1}{1 + e^{-(3.288 \times \text{FDG} + 1.245 \times \text{ASL} + 0.018 \times K_{trans} - 0.032 \times V_p - 5.571)}}$$

The result seemed to correspond generally well to the true FMISO maps on that point they both show higher value in the peripheral area of the tumor. However, the inside of tumor is not colored in the generated prediction map unlike the true ^{18}F-FMISO map. The cerebral cortex (especially in the frontal lobes) and basal ganglia were also colored FMISO-positive and this is supposedly caused by the high values of both FDG and ASL. High value in the basal ganglia is also seen and it apparently resulted from high value of FDG. The right side (opposite side to the tumor) is more remarkable than the left side, probably due to less uptake of FDG in the left side due to perifocal edema.

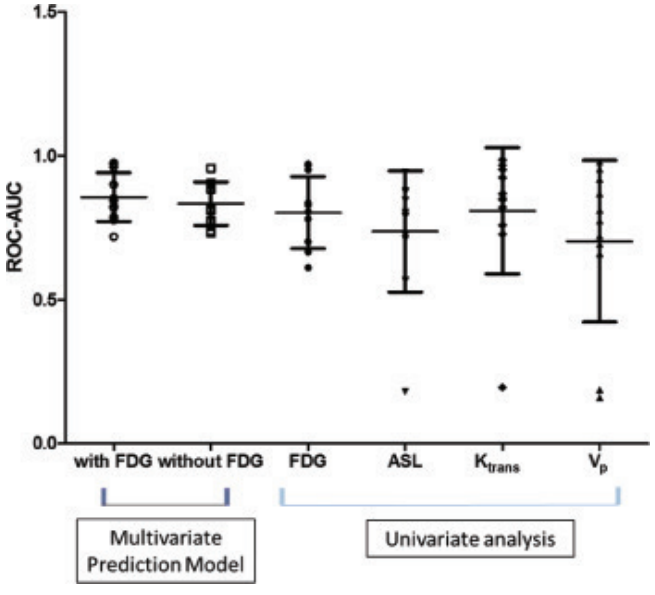

Fig. 2 Dot plot showing the areas under the receiver-operating characteristic curves. The average AUCs are shown with error bars or the standard deviation. The highest AUC is seen in the multivariate prediction model with FDG followed by the model without FDG. Note that there were no ASL, K_{trans}, and V_p outliers in the multivariate prediction models with or without FDG seen in the univariate analysis. FDG, ^{18}F-fluorodeoxyglucose; ASL, arterial spin labeling; AUC, area under the curve; ROC, receiver-operating characteristic..

Discussion

We have successfully generated a multivariate logistic regression model using MRI parameters and FDG accumulation to predict accumulation of FMISO. The prediction performance of both models with and without FDG was higher than of FDG, ASL, K_{trans}, and V_p in univariate analyses, suggesting that the multivariate model was effective for prediction of accumulation of FMISO.

The ability to predict FMISO positivity using MRI would be beneficial for many institutions, given the limited availability of FMISO and other agents that can visualize hypoxia. The method we developed not only predicted FMISO positivity in patients but also successfully generated a prediction map; moreover, the spatial distribution of FMISO positivity could be confirmed visually. This prediction map can be useful for determination of where to perform a biopsy, given that an FMISO-positive area is considered to be more malignant. It would help with identification of radioresistant hypoxic areas before starting radiotherapy, which would optimize the planning strategy.[17]

^{18}F-FMISO PET is also thought to be useful for assessment of the response to treatment, such as radiation combined with temozolomide or bevacizumab for high-grade glioma, and for detecting changes in oxygenation, so the prediction map might be suitable for that purpose.[18,19]

Although the cerebral cortex and basal ganglia were shown on the prediction map, these areas are easily recognized as normal structures by their shape, and can be excluded when we see a FLAIR image that shows the rough boundary of the tumor.

The prediction model with FDG had significantly better prediction performance than ASL and V_p in univariate analysis; however, the findings for the model without FDG did not reach statistical significance. Therefore, we assumed that FDG should be included in the multivariate prediction model when available, but that similar prediction performance can be achieved even without FDG.

The prediction performance of the model with FDG may be better explained by following mechanism: most malignant tumors tend to be hypoxic because of an imbalance between oxygen supply and demand, leading to a limited supply of oxygen to internal tumor tissues. Hypoxia causes several metabolic alterations, among which is increased glucose uptake. Transcription of hypoxia-inducible factor-1 alpha (HIF-1α), which survives only in hypoxic cells, leads to altered expression of several glycolytic genes and glucose transporters, which causes increased glucose uptake by tumor cells.[13] Thus, accelerated glucose uptake, shown as high accumulation of FDG, represents part of the hypoxic change in a tumor.

When it comes to considering relation between hypoxia and vascular abnormality, oxygen delivery is decreased beyond its diffusion distance under the circumstances where tumor proliferation proceeds at a greater rate than vascular development. Hypoxia promotes neovascularization through

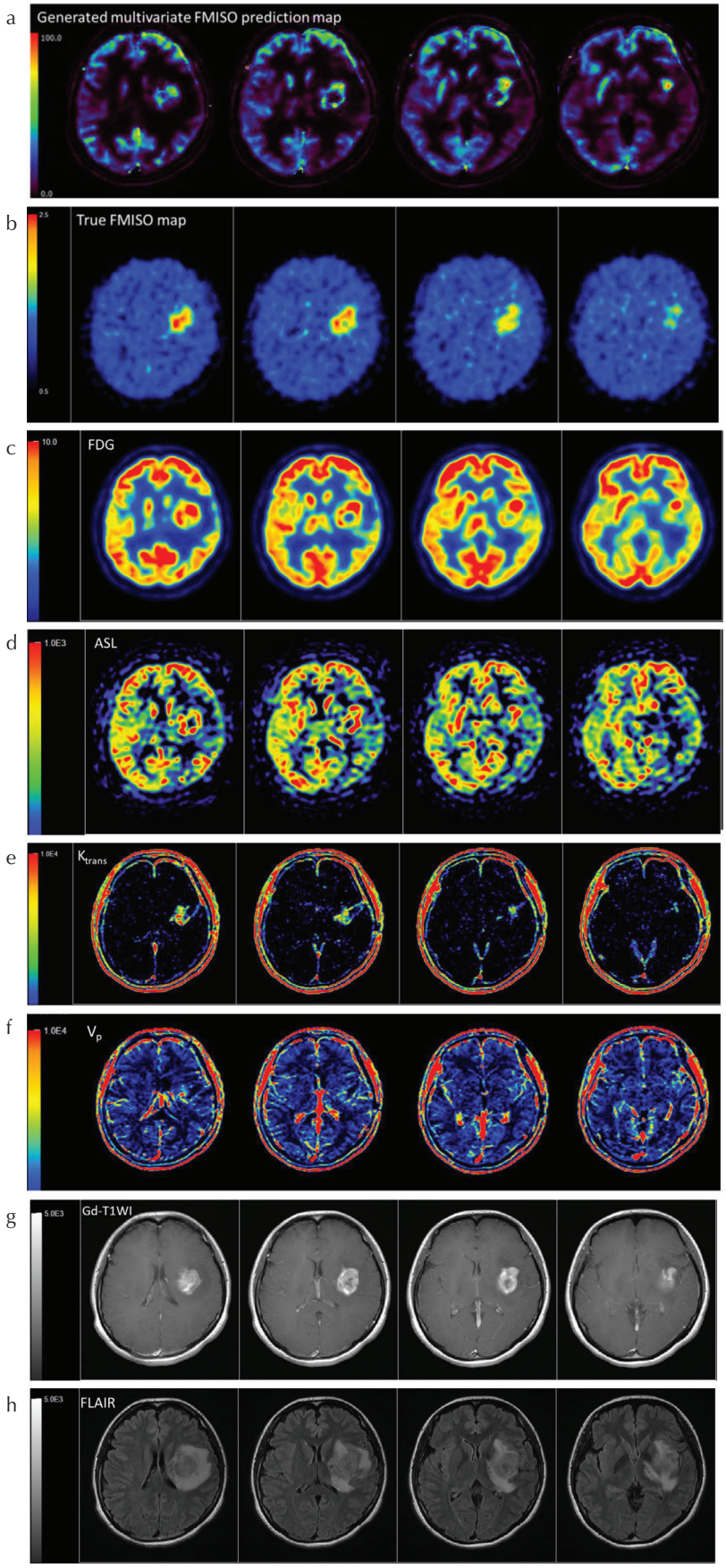

Fig. 3 Prediction maps (**a**), true FMISO maps (**b**), FDG (**c**), ASL (**d**), K_{trans} (**e**), V_p (**f**), contrast-enhanced T_1-weighted images (**g**), and FLAIR images (**h**) for case 6. The area with high FMISO values in the multivariate prediction model corresponds generally well to the true FMISO maps. Although high values are also seen on the prediction maps of the frontal cerebral cortex and basal ganglia (false-positive areas), these areas are easily excluded from the tumor on FLAIR images. FLAIR, fluid-attenuated inversion recovery; FMISO, ^{18}F-fluoromisonidazole; FDG, ^{18}F-fluorodeoxyglucose; ASL, arterial spin labeling.

a variety of molecular signals. HIF-1α, abovementioned, activates the transcription of many genes that help a tumor to survive in hypoxic conditions, including vascular endothelial growth factor, leading to the angiogenic cascade.[20,21]

A previous study in patients with newly diagnosed glioblastoma reported that there was a moderate positive correlation between blood flow and degree of hypoxia as measured by FMISO PET, and that higher FMISO accumulation and elevated level of vascular markers (K_{trans}, blood volume, and blood flow) at baseline were significantly associated with poor patient survival, although the correlations between the other pairs of hypoxic markers (such as FMISO the peak standardized uptake value (SUV_{peak}) or hypoxic volume) and vascular markers (such as K_{trans}, blood volume, or blood flow) were not statistically significant. It is suggested that inefficient tumor perfusion and increased vascular permeability because of abnormal tumor vasculature appear to drive tumor malignancy and contributing to tumor hypoxia in patients with newly diagnosed glioblastoma.[11]

Multivariate analysis could help to analyze various types of tumors. In our present study, most of the patients had glioma, but even with glioma (no. 10) ASL and V_p were seen to be outliers in univariate analysis. One of the patients had germinoma (case 8), with AUCs of 0.195 for K_{trans} and 0.161 for V_p. Even in the patient with germinoma, our multivariate prediction model showed AUCs of 0.824 (with FDG) and 0.773 (without FDG). The histopathological structure of germinoma and glioma are different; however, our multivariate prediction model might work well even in this patient with germinoma.

This study has several limitations. First, the number of the patients was small, which reflects the availability of FMISO PET, even with our institution. If we could have increased the number of patients, our multivariate prediction model without FDG might have demonstrated a significant difference in univariate analysis similar to that in the model with FDG. Furthermore, if we could obtain more patients, deep learning and other artificial intelligence could be applied to obtain a prediction model that is better than multivariate logistic regression. Second, most of our study subjects had glioblastoma, and the number of other types of brain tumor was small. Therefore, our prediction model needs to be validated in a wider variety of tumors. Third, ASL was used to estimate tumor blood flow; however, DSC perfusion is more commonly used to obtain blood flow, and blood volume can be obtained simultaneously. However, we wanted to include permeability in our prediction model, so gadolinium contrast was used for DCE. It was difficult to perform two gadolinium-enhanced studies at once, considering signal-to-noise ratio and contrast of images (as the amount of gadolinium contrast would become half); therefore, we chose ASL for estimation of blood flow, and blood volume was estimated by the V_p on DCE images. Fourth, we used the average values of the both hemispheres of cerebellum as the standard FMISO uptake. This method cannot be applied to the cerebellar tumors; however, the ROIs can be placed in skeletal muscles for the standard FMISO values, as is often the case with head and neck tumors.

Conclusion

A multivariate prediction model using blood flow, vascular permeability, and glycometabolism data can predict FMISO positivity in brain tumors.

Acknowledgment

This work was partly supported by Bayer AG.

Conflicts of Interest

The authors declare that they have no conflicts of interest.

References

1. Lee CT, Boss MK, Dewhirst MW. Imaging tumor hypoxia to advance radiation oncology. Antioxid Redox Signal 2014; 21:313–337.
2. Dewhirst MW, Cao Y, Moeller B. Cycling hypoxia and free radicals regulate angiogenesis and radiotherapy response. Nat Rev Cancer 2008; 8:425–437.
3. Gerstner ER, Zhang Z, Fink JR, et al. ACRIN 6684: assessment of tumor hypoxia in newly diagnosed glioblastoma using ^{18}F-FMISO PET and MRI. Clin Cancer Res 2016; 22: 5079–5086.
4. Kobayashi H, Hirata K, Yamaguchi S, Terasaka S, Shiga T, Houkin K. Usefulness of FMISO-PET for glioma analysis. Neurol Med Chir (Tokyo) 2013; 53:773–778.
5. Hirata K, Terasaka S, Shiga T, et al. ^{18}F-fluoromisonidazole positron emission tomography may differentiate glioblastoma multiforme from less malignant gliomas. Eur J Nucl Med Mol Imaging 2012; 39:760–770.
6. Spence AM, Muzi M, Swanson KR, et al. Regional hypoxia in glioblastoma multiforme quantified with [18F] fluoromisonidazole positron emission tomography before radiotherapy: correlation with time to progression and survival. Clin Cancer Res 2008; 14:2623–2630.
7. Toyonaga T, Yamaguchi S, Hirata K, et al. Hypoxic glucose metabolism in glioblastoma as a potential prognostic factor. Eur J Nucl Med Mol Imaging 2017; 44:611–619.
8. Bekaert L, Valable S, Lechapt-Zalcman E, et al. [18F]-FMISO PET study of hypoxia in gliomas before surgery: correlation with molecular markers of hypoxia and angiogenesis. Eur J Nucl Med Mol Imaging 2017; 44:1383–1392.
9. Law M, Yang S, Babb JS, et al. Comparison of cerebral blood volume and vascular permeability from dynamic susceptibility contrast-enhanced perfusion MR imaging with glioma grade. AJNR Am J Neuroradiol 2004; 25:746–755.
10. Roberts HC, Roberts TP, Brasch RC, Dillon WP. Quantitative measurement of microvascular permeability in human brain tumors achieved using dynamic contrast-enhanced MR imaging: correlation with histologic grade. AJNR Am J Neuroradiol 2000; 21:891–899.
11. Shiroishi MS, Habibi M, Rajderkar D, et al. Perfusion and permeability MR imaging of gliomas. Technol Cancer Res Treat 2011; 10:59–71.
12. Colliez F, Fruytier AC, Magat J, et al. Monitoring combretastatin A4-induced tumor hypoxia and hemodynamic changes

using endogenous MR contrast and DCE-MRI. Magn Reson Med 2016; 75:866–872.
13. Ellingsen C, Hompland T, Galappathi K, Mathiesen B, Rofstad EK. DCE-MRI of the hypoxic fraction, radioresponsiveness, and metastatic propensity of cervical carcinoma xenografts. Radiother Oncol 2014; 110: 335–341.
14. Ponte KF, Berro DH, Collet S, et al. In vivo relationship between hypoxia and angiogenesis in human glioblastoma: a multimodal imaging study. J Nucl Med 2017; 58: 1574–1579.
15. Rajendran JG, Mankoff DA, O'Sullivan F, et al. Hypoxia and glucose metabolism in malignant tumors: evaluation by [^{18}F]-fluoromisonidazole and [^{18}F]-fluorodeoxyglucose positron emission tomography imaging. Clin Cancer Res 2004; 10:2245–2252.
16. Alsop DC, Detre JA, Golay X, et al. Recommended implementation of arterial spin-labeled perfusion MRI for clinical applications: a consensus of the ISMRM perfusion study group and the European consortium for ASL in dementia. Magn Reson Med 2015; 73:102–116.
17. Herholz K. Brain tumors: an update on clinical PET research in gliomas. Semin Nucl Med 2017; 47:5–17.
18. Yamaguchi S, Hirata K, Toyonaga T, et al. Change in ^{18}F-fluoromisonidazole PET Is an early predictor of the prognosis in the patients with recurrent high-grade glioma receiving bevacizumab treatment. PLoS One 2016; 11:e0167917.
19. Bell C, Dowson N, Fay M, et al. Hypoxia imaging in gliomas with ^{18}F-fluoromisonidazole PET: toward clinical translation. Semin Nucl Med 2015; 45:136–150.
20. Swanson KR, Chakraborty G, Wang CH, et al. Complementary but distinct roles for MRI and ^{18}F-fluoromisonidazole PET in the assessment of human glioblastomas. J Nucl Med 2009; 50:36–44.
21. Jain RK, di Tomaso E, Duda DG, Loeffler JS, Sorensen AG, Batchelor TT. Angiogenesis in brain tumors. Nat Rev Neurosci 2007; 8:610–622.